Proceedings of ASME Turbo Expo 2015
GT2015
June 15-19, 2015, Montreal, Canada

GT2015-43150

EXPERIMENTAL VALIDATION OF A MESH QUALITY OPTIMIZED MORPHED GEOMETRIC MISTUNING MODEL

Alexander A. Kaszynski
Universal Technology Corporation
Dayton, OH 45434
Email: akascap@gmail.com

Joseph A. Beck
Jeffrey M. Brown
Turbine Engine Division
U.S. Air Force Research Laboratory
Wright-Patterson AFB, OH 45431

ABSTRACT

High cycle fatigue due to mode localization caused by geometric and material mistuning is one of the leading failure risks of integrally bladed rotors (IBRs). Due to the computational analysis cost of full wheel models, IBR mistuned response amplifications are often modeled with reduced order models (ROMs). However, many developed ROMs are based on nominal mode assumptions that do not consider mode shape variations that have been shown to impact predicted mistuned response. Geometrically mistuned finite element models (FEMs) do account for mode shape variations but are notoriously difficult to construct and analyze. Recent advancements in optical scanning have enabled the rapid acquisition of highly accurate dense point clouds representative of manufactured hardware. Previous research pioneered a novel method to automatically and robustly construct an FEM directly from tessellated scan data, this research adds new mesh quality verification algorithms and experimentally validates this algorithm using results from traveling wave excitation. Sensitivity to mesh and point cloud density are also assessed to determine a best practice for creation of the as manufactured mistuned rotor model.

NOMENCLATURE

CMM	Coordinate measuring machine
DOF	Degrees of freedom
FEA	Finite element analysis
FEM	Finite element model
FMM ID	Fundamental mistuning model identification
FRF	Frequency response function
GMM	Geometrically mistuned model
IBR	Integrally bladed rotor
ICP	Iterative closest point
ISA	Iterative spring analogy
MORPH	Automated mesh morphing algorithm
R	Pearson Correlation Coefficient
RBF	Radial basis function
ROM	Reduced order model
TSD	Tessellated scan data
TWE	Traveling wave excitation

INTRODUCTION

A major breakthrough in engine design practice has been incorporating integrally bladed rotors (IBRs) into the current generation of aircraft engines. IBRs have the advantages of removing design and production challenges associated with inserted blades which then leads to significant improvements in aerodynamic efficiency. The improvements of an IBR come at a cost; removal of the frictional damping at inserted blade contact surfaces can increase the risk of response amplification due to a phenomenon known as mistuning [1]. Mistuning is caused by the blade to blade variations in material and geometry that are inherent to manufacturing processes. Mistuning is a significant problem in the engine industry as the response amplification can

be as high as three times the tuned blade response and can lead to blade failure due to high cycle fatigue (HCF). In fact, as much as 30% of jet fighter maintenance costs for the US Air Force have been due to HCF [1]. The quantification and prediction of mistuning is a necessity in reducing maintenance cost as well as increasing aircraft reliability in current and next-generation aircraft.

Mistuning has been studied for over half a century and significant progress in understanding its behavior has been made. Several recent activities have used finite element methods and reduced order models (ROMs) to predict mistuned response. ROMs have been pursued because of the nature of mistuned IBRs, which require full wheel models that could contain on the order of 10^6 or greater degrees of freedom (DOF). Such models restrict the exploration of the design space and make probabilistic calculations intractable. Initial ROM developments assumed nominal mode behavior, that is, airfoil geometry variations impacted airfoil frequencies, but not mode shape [2, 3]. More recently, researchers have developed ROMs that explicitly account for airfoil geometry deviations using both frequency and mode shape variation [4–6]. These efforts have demonstrated significant differences between the nominal and non-nominal mode approximation approaches which has motivated continued research in geometric mistuning models (GMMs).

Use of GMMs incur the challenge of efficiently collecting airfoil geometry and accurately converting such data into a finite element model (FEM). Fortunately with the advent of high accuracy optical scanners, it is now possible to fully represent an as-manufactured parts as detailed point clouds of geometric information. In prior work, a method named MORPH [7] was developed that used these high density point clouds to semi-automatically reverse engineer a GMM viable for mistuned FEA. The optical geometry measurement approach has been found to be superior to models constructed from traditional touch probe systems that have difficulty accurately measuring the fillet regions of airfoils.

The prior effort on MORPH specifically dealt with the process and rapidity of the GMM generation. This paper describes additional advancements in the robustness of the MORPH algorithm as well as its experimental validation using traveling wave excitation (TWE) data collected from a production IBR. An analysis of mesh convergence, optical scanner noise, and point cloud alignment will also demonstrate the sensitivity of the MORPH process to the experimental results. The experimental results are post-processed with the fundamental mistuning model identification method (FMM ID) [8, 9]. The research presented here shows novel evidence using FMM ID that a GMM created using MORPH can indeed accurately represent as-manufactured turbomachinery in the digital realm.

This paper continues by briefly describing the original MORPH algorithm. Next, a convergence study using the original algorithm compared to experimental data is discussed, resulting in the determination of improvements to the algorithm. Two sensitivity studies follow to evaluate the effectiveness of the registration algorithm and to bound minimum alignment criteria between the collected scan data and the FEM. It will be shown that MORPH, even before implementing the improvements found in the convergence study, is sensitive enough to capture the minute variations between blades in an as-manufactured IBR as shown by its comparison to experimental results.

ORIGINAL ALGORITHM

Prior to development of MORPH, an algorithm called semi automated blade reverse engineering (SABRE) was developed that parametrically modified geometry of an existing FEM to make it match geometric data obtained by modern optical white light scanners [10]. A challenge of SABRE, was the requirement for parametric geometry that could use standard hexahedral mesh generation tools. This required significant effort from an expert analyst for each new IBR to be studied. Future work would also show that the parametric geometry approach was overly constraining at the fillet, tip, and other regions and would not precisely fit collected point cloud data. Because of this, a mesh morphing process was developed called MORPH.

MORPH directly moves the nodes on the surface of a FEM using an intelligent neural network model between the FEM and the TSD. MORPH requires an initial nominal FEM of reasonable accuracy to begin the mesh morphing process. This "seed" model is a nominal tuned approximation of the mistuned IBR and can come from either an existing model from the design process or a model reverse engineered from an optically measured rotors tessellated scan data (TSD). Once generated, the surface nodes are to be moved towards the TSD, which as it turns out, incurs its own set of challenges.

While early attempts at mesh morphing were reasonably successful by moving modes directly along normals projected from surface FEM nodes, this approach was prone to several modes of failure, to include the generation of corrupt elements due to high surface displacements, poor internal element quality, and the inability to capture highly misaligned portions of the IBR. The problem was two-fold, geometry capture cannot be improved by the inflation or deflation of the FEM, and the quality of the FEM must be maintained by updating interior nodes in an intelligent fashion. After attempting several approaches, the optimal method was determined to be an iterative neural network based approach. The original algorithm follows:

1. Compute FEM surface node normal vectors and determine distance from the FEM nodes to the TSD using algorithm presented in [11]. Each FEM node normal N is defined by origin O, location of the node, and direction D representing the normal vector of that node as shown below in Equation

(1)

$$N(t) = O + tD \tag{1}$$

2. Calculate node displacement vectors using a neural network based alignment approach with network scoring based on FEM node to TSD face distance and alignment. A vector of scores S is computed by

$$S = \frac{d_{\min}\frac{1}{d_f} + \hat{n}_f \cdot \hat{n}_n}{2} \tag{2}$$

where d_f is a vector of the distances between the FEM node and the center of adjacent TSD faces normalized by factor $d_{\min}$, $\hat{n}_f$ is the normal vector extending from a tessellated face of the TSD, and $\hat{n}_n$ is a node normal vector from node n extending from the FEM.

3. Distribute the local node displacements among adjacent nodes using a radial basis function (RBF), thereby allowing nodes to influence their neighbors through the Gaussian RBF φ. The node-to-node influence is dependent on the geodesic distance between two nodes through the 3D FEM and is given by

$$\varphi(r) = \tau e^{-(\varepsilon r)^2} \tag{3}$$

where τ is the linear influence coefficient, ε is the exponential influence coefficient, and r is the geodesic distance through the 3D mesh.

4. Sum the RBF displacement vectors for all nodes and update node positions. Limit maximum node movement by a fraction of the global average element edge length.
5. Check updated element shape. Limit node movements that would corrupt surface elements (e.g. aspect ratio and skew).
6. Iterate through steps 1-4 and modify the RBF based on the rate of change of node positions. Run until FEM to TSD distance converges.
7. Place surface mid-side nodes of quadratic elements between edge nodes. Compute mid-side node normal vectors based on the average of the edge node vectors and move those nodes directly along the normal vectors to the TSD.
8. Update the positions of internal nodes using the iterative spring analogy (ISA)

MORPH ALGORITHM IMPROVEMENTS

The algorithm presented in the previous section proved to be sufficiently robust to generate volumetrically accurate FEMs from academic IBRs, but was found to be prone to error when applied to non-academic IBRs. The academic rotor had thick low aspect ratio blades that were particularly suited to MORPH. When applied to other as-manufactured IBRs, the analytical models generated from MORPH demonstrated a weaker than expected agreement to experimental data and in some cases failed to produce a valid FEM. As it will be shown, the original algorithm can fail to maintain sufficient element quality during MORPH and this leads to inaccurate results. It is important to specify that the element quality in the prior method did meet conventional quality criteria, but this quality was found to be insufficient for comparison to the experimental mistuning data. Additionally, with high aspect ratio blades, minor nicks in the IBR as well as noise in the scan data due to the razor thin trailing edges could cause the original MORPH to generate invalid elements during the node updating process. To correct for the limitations of the original algorithm, this section presents three major improvements to eliminate mesh quality variation between blades, control node movements during MORPH to limit mesh corruption, and correct invalid elements to guarantee a valid mesh.

Measuring Mesh Quality with the Mean Ratio Quality Metric

The basis for the finite element method is the discretization of a continuous domain into a system of elements for a solution pertaining to the original domain. The solution of the FEM relies on a well conditioned stiffness matrix which can become ill-conditioned when the gradient at finite element interpolation points is inaccurate because of high variance between the actual and ideal element. In the case of this research, an ideal hexahedral is an equilateral cube. While rotation and size have no effect on gradient computation, the hexahedral element is sensitive to skew and face warping, and to a lesser degree, aspect ratio. The original MORPH algorithm only included a rudimentary element checking scheme utilized by the applied commercial meshing software; the Jacobian ratio is evaluated at the interpolation point for each element. While this is an effective method to ensure that the mesh output from MORPH is solvable in FEA, it does nothing to report on quality of the mesh, the variance in mesh quality between blades, or to repair corrupt and invalid elements.

In order to qualify the change in mesh quality due to surface node displacement as well as determine invalid elements, the mean ratio quality metric [12] was selected. It was selected due to its established use within the meshing and research community [13, 14] and particularly for its applicability to all FEM element types. The mean ratio quality metric is based on measuring the deviation of an element from its ideal shape and is well suited for determining the pre and post MORPH state of a mesh given external node displacements. The mean-ratio element quality metric begins by creating simplexes at each node of a hexahedral. First, a 3×3 matrix is produced where the spanning edge vector for each simplex is determined by

$$D_k = (P_{N_{k,2}} - P_{N_{k,1}}, P_{N_{k,3}} - P_{N_{k,1}}, P_{N_{k,4}} - P_{N_{k,1}}) \tag{4}$$

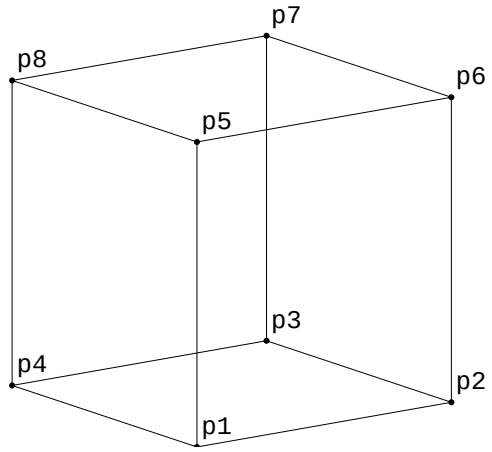

FIGURE 1: Hexahedral Element Numbering Scheme

for each node N and adjacent node k according to Table 1 given the standard hexahedral numbering scheme in Figure 1. Each 3×3 matrix is composed of three column vectors from the origin of node N to each adjacent node in the direction towards the adjacent nodes. The mean quality number $q(E)$ is then computed by

$$q(E) = \frac{1}{|N|} \sum_{k=1}^{|N|} \frac{3|(D_k^{2/3})|}{||D_k||_F} \tag{5}$$

where $||D_k||_F$ is the Frobenius Norm operator. An ideal simplex would be a 3×3 identity matrix since each simplex vector set would be orthogonal and of equal length, which is the definition of the ideal element. As the aspect ratio or skewing of the hexahedral element increases, the mean quality ratio decreases as the edge vectors extending from each node will be less orthogonal or of different lengths thereby decreasing the determinant of D_k while having a lesser effect on the Frobenius norm of D_k. Since the solution to a modal analysis is dependent on the quality of the elements composing a FEM, mesh quality variation between blades due to semi-organized node displacement can have drastic effect on the accuracy of the mistuned model. Given that the average blade to blade mistuning can be as small as $\pm$ 0.25%, small variations in mesh quality is sufficient to vary blade alone natural frequency and the predicted mistuned response amplification. Given that an improved quality metric is applied, the next step is to correct for element corruption due to surface node movements.

TABLE 1: Hexahedral Node Simplex Numbering Scheme

Simplex	Nodes			
1	1	4	5	2
2	2	1	6	3
3	3	2	6	4
4	4	3	8	1
5	5	8	6	1
6	6	5	7	2
7	7	6	8	3
8	8	7	5	4

Element Optimization through the Geometric Element Transformation Method

The ISA used in the initial version of MORPH, while straightforward in its implementation on a FEM given surface displacements, is insufficient for the maintenance of high element quality. The FEA realm is prolific with mesh optimization schemes, from the simple Laplacian smoothing technique [15] to complex global mesh optimization schemes such as the target matrix transformation method [16]. Several optimization algorithms were attempted in order to post-process the morphed mesh and eliminate mesh quality variance. The geometric element transformation method (GETMe) [17] was selected as a candidate due to its iterative, rapid, and parallel nature which is most applicable to large degree of freedom FEMs. One of the main advantages of GETMe over other potential smoothing optimization algorithms was its ability to operate independently of boundary conditions. Whereas global optimization algorithms, and even Laplacian Smoothing, necessitate fixing surface nodes and freezing potentially corrupt surface elements, GETMe allows for the optimization of surface adjacent elements. For example, during extreme nodal displacements when accounting for severe discrepancies between the seed model and the optical scan data, surface elements can be warped to such a high degree as to create invalid elements despite the spreading of surface nodal displacements through a Gaussian radial basis function. Thus, GETMe was chosen to repair elements on the surface of the FEM that would be impossible to repair with an optimization-based mesher.

Fundamentally, GETMe operates by creating a dual element and then projecting key features of that dual element out to recreate the original element. While this mesh optimization approach supports mixed element types, this paper will focus on the opti-

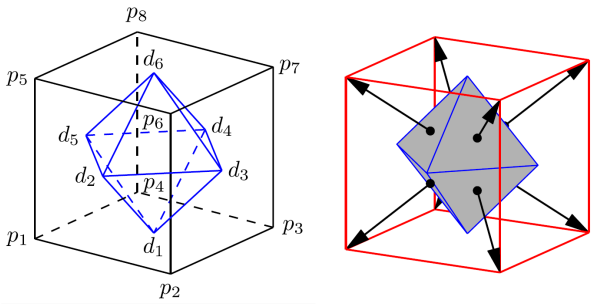

FIGURE 2: GETMe: Hexahedral Dual Element

mization of a hexahedral as it has been selected as the optimal element for mistuning prediction. The dual element is shown in Figure 2 and the octahedron in this case begins by computing the center point of each face of the hexahedral. Using the standard hexahedral element numbering scheme these center points are shown in Table 2. The octahedron faces are then assembled by connecting the face center-points by the numbering scheme in Table 3.

TABLE 2: Hexahedral Face Numbering Scheme

Face	Nodes			
1	1	2	3	4
2	1	2	6	5
3	2	3	7	6
4	3	4	8	7
5	4	1	5	8
6	5	8	7	6

TABLE 3: Octahedron Node Numbering Scheme

Node	Face		
1	1	2	5
2	1	3	2
3	1	4	3
4	1	5	4
5	6	5	4
6	6	2	3
7	6	3	4
8	6	4	5

The key feature of GETMe is the reconstruction of the new hexahedral based upon normal vectors from the dual element faces given by

$$n_k = \frac{1}{2}(d_{\overline{F}_{k,3}} - d_{\overline{F}_{k,1}}) \times (d_{\overline{F}_{k,4}} - d_{\overline{F}_{k,2}}) \tag{6}$$

where the base point for each normal vector is the center-point of the corresponding dual element face. At this step in the optimization process each element has a corresponding more optimal element. Since each node is generally connected to more than one element, the optimized nodal positions are computed using a weighted average computed by summing each more optimal node position with a nodal weighting given by

$$w_j = (1 - q(E_j))^{\eta} \tag{7}$$

where $q(E_j)$ is the mean ratio of that element and η is a user selected exponent. For bladed structures, $\eta = 5$ was selected to give a high priority to lower quality elements. GETMe was first implemented in parallel using MATLAB given the ease of implementing matrix wide binary operations without the use of loops after displacing surface node movements. GETMe was then implemented in a localized error correction routine after detecting invalid elements given by any element with an imaginary component in the determinant of Equation 4. The parameter E_j in Equation 7 was set to the Boolean value of the imaginary component of the determinant of 4, thereby giving full priority to invalid elements.

The speed at which an element transformed into its ideal counterpart, or regularization speed, was controlled by taking the weighted average of the original element and its transformed counterpart. In order to ensure elements surrounding invalid elements were not invalided due to localized optimizing as well as limiting surface node misalignment the localized parallel implementation of GETMe gave a small weight to the new more ideal element. In order to limit the computation time for full parallel implementation of GETMe, the transformed elements were given a high priority and the original elements a low priority.

To limit the total number of iterations, GETMe was implemented in conjunction with the ISA along with the original neural network based algorithm. Without modifying the core of the original algorithm, the new error checking/correction procedure follows:

1. Run a single step of neural network based FEM/TSD matching. Advance to step 3 if nodal displacements are below a threshold. Otherwise:
   (a) Compute mesh quality and check for any inverted elements. If none are detected return to called step. Otherwise:
   (b) Run ISA and propagate external node movements to interior nodes. Recheck elements for invalid elements. If none are detected return to called step. Otherwise:
   (c) Identify nodes belonging to invalid elements. Zero out those node displacements but do not freeze these nodes. These nodes will still be effected by surrounding nodes due to the Gaussian RBFs. Recompute node displacements. Recheck element quality and return to called step if all elements are valid. Otherwise:
   (d) Run GETMe only on invalid nodes. Mesh validity will be maintained at the expense of the geometric accuracy of the FEM. Return to called step.
2. Move nodes directly along node normals to the surface of the TSD and run run error checking algorithm in step 1. Proceed to step 3 when the surface of the FEM and TSD distance remains constant within a certain threshold.
3. Run the paralleled GETMe algorithm. At the end of every

step, revert surface nodes to their original location and check element quality. Revert invalid elements to their original location.

This new algorithm was combined with the original code and implemented in the following section. As it will be shown, the additional error checking steps added to MORPH not only allow for mesh metamorphosis without corrupting the FEM, but enable sufficient FEA accuracy to allow for precise mistuning predictions for an IBR.

MORPH VALIDATION

Three investigative studies were conducted to determine the accuracy of MORPH in producing an accurate 360° mistuned FEM of an as-manufactured rotor. The IBR chosen for this study was a 22 blade production IBR. Early assessments in the accuracy in MORPH compared the volumetric accuracy of MORPH to alternative reverse engineering methods but stopped short of actually determining the relative sector mistuning of the model. As mistuning is primarily driven by variations in sector frequencies [4], three studies were chosen to determine the accuracy of the MORPH based GMM by comparing it to experimental results obtained from TWE experiments: A multivariable convergence study, noise sensitivity study, and alignment sensitivity test.

Basis for Experimental Validation

Fundamental mistuning model identification, or FMM ID, allows for the determination of sector to sector deviation from for a single isolated modal family (i.e. 1^{st} bend (1B), 2^{nd} bend (2B), 1^{st} torsional (1T), etc.) [8]. As FMM ID is most accurate with mode families with low disk participation the 1T mode family from the IBR was chosen for analysis. This was verified by an analytical analysis that shows most of the mode's strain energy is confined to the blades. Experimental data was obtained through the use of a TWE system. Details on the exact operation of the TWE can be obtained from [18], but in short, the TWE replicates engine order EO excitations by forcing blades in a phase pattern matching the excitation pattern expected from engine configuration or flow path conditions. For example, 4 inlet guide vanes upstream of the IBR would create an EO excitation of 4. In a perfectly tuned 22 bladed rotor the system would respond with nodal diameter (ND) 4, with 4 nodal lines extending from the centroid of the IBR. The blades on either side of the nodal lines are 90° out of phase with one another and this ND pattern creates 8 separate phase groups. However, in a non-ideal rotor mistuning breaks down the periodicity of the IBR and distributes the modal energy to alternate NDs making it impossible to directly infer the tuned characteristics of the IBR.

FMM ID allows for the engineer to calculate the relative sector to sector mistuning for an isolated mode family through a least squares fit of the system mode shapes and frequency data. FMM ID is particularly suited for the 1T system mode due to its low disk participation and low sensor noise due to the test sensor setup for the TWE. The TWE was setup to measure the 1T system mode by placing magnets on the trailing edge of each of the IBR's blade tips and exciting them using calibrated inputs at the EO of interest. Due to the characteristics of this system mode and the mistuning of the IBR, EO 4 was selected to excite the rotor to disperse modal energy to all NDs to aid in FMM ID. The rotor was then excited over a frequency range that encompassed the IBR's response at ND 0 through 11. The frequency response function (FRF) was then recorded for each blade and the IBR's system modes at 1T were identified by combining the responses of all blades and selecting the strongest peaks of the resulting FRF. Each peak corresponds to a system mode and the relative blade deflections at each system mode describe the mode shape of the IBR. The mode shapes and frequencies of each system mode were then inputted into FMM ID to determine the relative sector to sector mistuning and tuned system frequencies. IBR sector mistuning ratios and the IBR tuned system frequencies are the two key inputs for determining blade amplification and will be compared to the analytical results from the MORPH based GMM.

The GMM was generated by collecting optical scan data from the as-manufactured IBR, generating a nominal tuned CAD/FEM of the IBR, and MORPHing the nominal FEM to the optical scan data in order produce a fully mistuned model. The optical scan data was collected through the use of a commercial structured light optical scanner using a small scan volume ($170 \times 170 \times 170$ mm) in order to fully capture the leading and trailing edges of the IBR. A nominal CAD model of a cyclic sector was created using parametric reverse engineering software. The single cyclic sector model was then meshed using commercial meshing software with quadratic hexahedrals to limit model size and increase mode shape accuracy. This was accomplished by separating the sector CAD into 6-sided cubical structures that could be meshed using traditional sweeping methods or volumetric mapped meshing. An all hexahedral model was used in order to decrease the occurrence of numerical mistuning between blades and also due to the adaptivity of a hexahedral mesh to the high aspect nature of blades as hexahedral shape functions are less sensitive to aspect ratio scaling than tetrahedral shape functions. The sector FEM was replicated 21 times about the axis of revolution (Z-axis) to produce a tuned 22 bladed 360° model which was then mistuned using MORPH. Each sector of the mistuned IBR contained an identical number of nodes and similar element shapes to ensure that sector mistuning was primarily due to changes in geometry rather than false numeric mistuning.

The initial mistuned FEM was kept at a low density in order to rapidly prototype a mistuned IBR and verify its correlation to the experimental results. This initial full FEM contained 185,416 nodes and 33,528 quadratic hexahedral elements. The disk was not mistuned due to the assumption that disk mistuning would

have a miniscule contribution to sector mistuning.

The geometry of the FEM was modified using both the original and the improved MORPH algorithm to produce GMMs of the production IBR. However, when implementing the original MORPH algorithm large node movements on the disk blade fillet corrupted internal elements and resulted in an invalid FEM. Figure 3 shows the nominal (dotted lines) and GMM from the new MORPH algorithm (solid patches) and this figure demonstrates that the node movements along the fillets along the FEM are quite drastic. Despite this, the new MORPH algorithm produced a well shaped FEM as indicated by Figure 3 where elements are colored by their mean quality ratio in which solid red indicates a mean ratio quality metric of zero and bright green indicates one. While elements on the leading and trailing edges have the lowest quality due to their high aspect ratios, hexahedral elements are well suited to high aspect ratios and this will have little effect on the solution of the FEM. More importantly, despite the large modification of the blade/disk fillet MORPH did not produce invalid or poorly shaped elements following the mesh metamorphosis. With a valid mistuned GMM the next step is to determine the relative sector mistuning deviations and compare it to the experimental results.

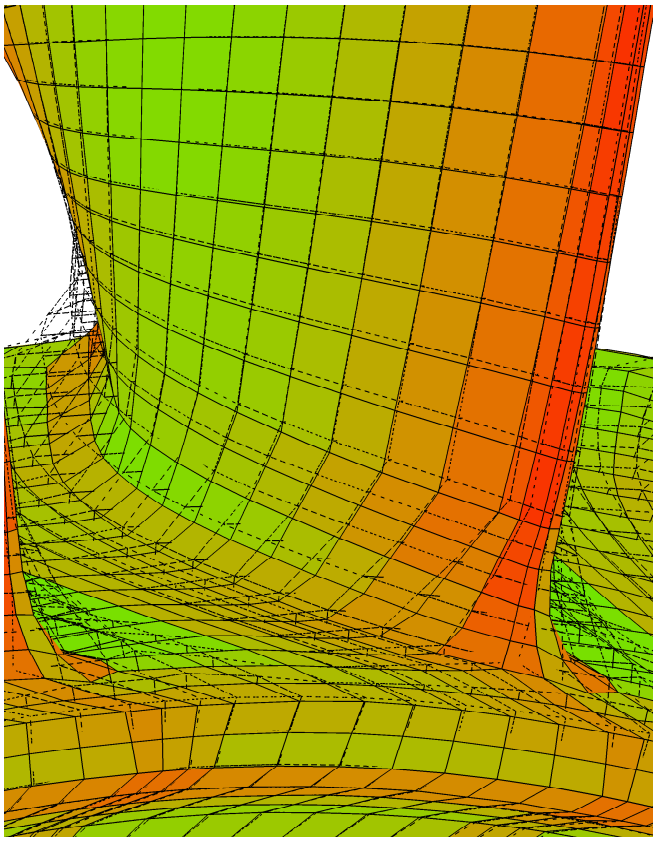

FIGURE 3: MORPHed GMM

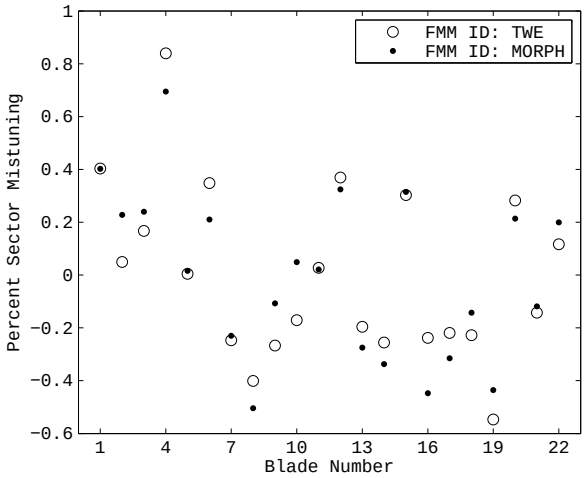

FIGURE 4: Production IBR Full FEM

As the IBR from the experimental analysis was placed on a isogrid elastomeric pad to simulate a free boundary condition, the analytical analysis replicated this by removing DOF constrains on the IBR and allowing the model to remain boundary condition free. The GMM's natural frequencies and mode shapes for 1T were computed from a boundary free modal analysis, but instead of inferring mode shapes from a FRF the mode shapes were directly outputted for each of the 22 mode shapes for the 1T family at the same measurement locations as in the TWE. This ensures a noiseless extraction of the IBR's mistuned system modes. The idealized tuned system modes and the relative sector variations were computed using FMM ID and an initial comparison between the analytical and experimental results can be found in Figure 4.

These initial results show a strong correlation between the two methods of analysis. The result is significant as this is the first ever validation of an optically measured point cloud-based GMM's accuracy using experimental results. This is an important milestone as it shows that in spite of experimental error, potential numerical mistuning, and numerical assumptions from FMM ID, the sector natural frequencies extracted from a family of mode shapes are well correlated to the experimental data. The remainder of this paper will indicate the accuracy of the GMMs based on the correlation between the relative sector mistuning ratios between the analytical and experimental results. The Pearson correlation coefficient is calculated by determining the covariance between the sector mistuning ratios from the GMM and the TWE in the numerator of

$$\rho(X,Y) = \frac{\mathbf{Cov}(X,Y)}{\sqrt{\mathbf{Var}(X)\mathbf{Var}(Y)}} \tag{8}$$

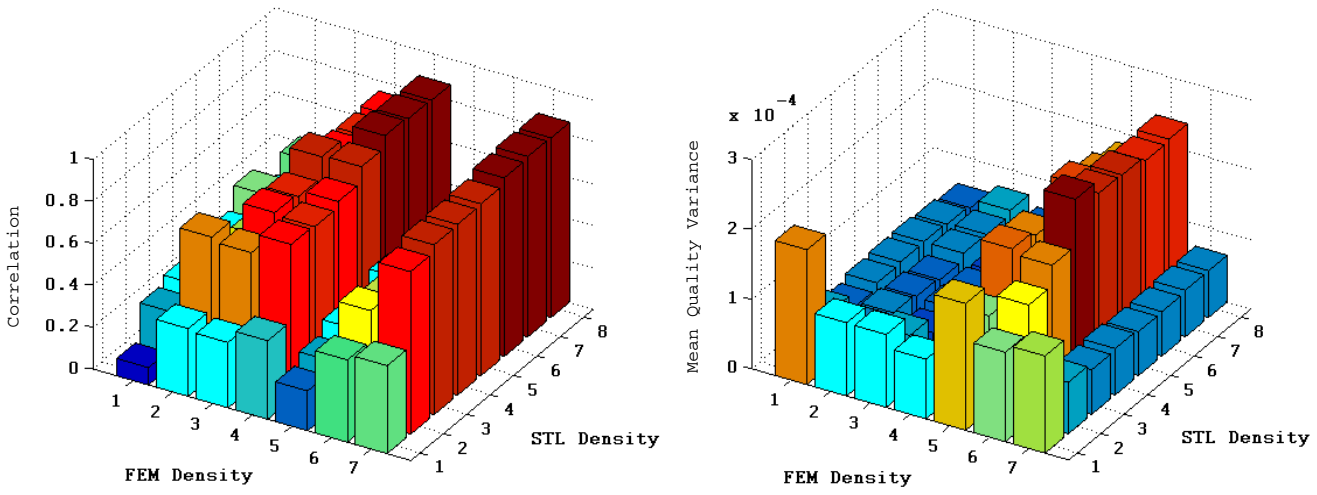

FIGURE 5: Correlation Convergence Study Results. Pearson Correlation Coefficient (Left), and Mean Element Ratio (Right)

and is normalized by the square root of the product of the variances in the denominator where X and Y correspond to the individual sector mistuning ratios from the GMM and TWE FMM ID results respectively. The correlation between the datasets in Figure 4 is 0.940 and will be referred to henceforth as R or as R^2 when the correlation coefficient is squared to emphasis variations across multiple datasets.

The following three sections will analyze the effect model and method variations have on the correlation between the FMM ID datasets. The purpose of the next three sections is to demonstrate the necessity of the newly introduced mesh quality code as well as the robustness of the MORPH algorithm for a wide variety of scenarios.

Multivariable Convergence Study

The minimization of discretization and interpolation error is a crucial step of FEA, and it is usually measured and minimized through a convergence study where the mean element edge length is varied to observe its effect on the solution of the FEM. As MORPH is dependent on both the density of the FEM as well as the TSD, this section shows the results of a multivariable convergence study where the density of the FEM and the TSD are varied to observe their effects on the analytical correlation to the experimental results.

In order to determine the sensitivity of the mistuned model to the resolution of the optical scan data, the original point cloud of approximately 8 million points was decimated to several smaller point clouds and then retessellated without modifying the original point locations. This was done so that noise was not introduced into the point cloud, though this is an issue that will be investigated later in this paper. The original CAD was also meshed at 7 different densities to determine the effect of mesh density on the mistuning convergence of the MORPH algorithm. The range of the FEM density was selected to reflect reasonable mesh sizes currently in use in modern FEA. Through trial and error, smaller FEMs were found to be insufficient to accurately represent an IBR while models denser than maximum FEM size were too large to run a convergence study without utilizing more computer resources. Table 4 shows the parameters of the multivariable convergence study in which 56 separate FEAs were run.

The first pass of the MORPH convergence study took place without the use of element shape optimization and only utilized the non parallel GETMe algorithm that corrected only the invalid elements. As shown on the left 3D bar plot of Figure 5 there is a strong correlation between TSD density and the correlation to the

TABLE 4: Convergence Study Parameters

TSD Density (Millions of Points) \ FEM DOF (Thousand)	166	264	330	405	696	873	1,198
0.20	#1	#2	#3	...			
0.34	#8	#9	...				
0.58	#15	...					
1.06	...						
1.93							
3.54							
6.53							
8.86							

experimental results. However, increasing FEM density did not guarantee a more accurate GMM given the low correlations of the medium density FEMs #5 and #6. Results from those GMMs reveal an important facet of geometric mesh metamorphosis: the effects of numeric mistuning on model accuracy. The results from FEMs 5 and 6 were initially perplexing as it is generally assumed that increasing mesh density increases analytical model accuracy due the reduction in discretization error. However, in this case artifacts in the mesh were introduced to these meshes to a greater degree than other FEMs because of the high aspect ratio of the elements in the center of the blade. As the number of elements through the blade could only be increased at integer increments, FEMs 5 and 6 had a large number of element divisions from the root up and a limited number through the blade. Therefore, relatively minor changes in the surface nodes had a much larger effect on element skewing despite the use of both surface and subsurface propagation algorithms (i.e. ISA, RBF). To verify that the loss in accuracy was in fact due to variation in mesh shape/quality between blades, element quality was tracked for each post-MORPHed model of the convergence study using the mean-ratio quality metric [19].

As shown on the right of Figure 5 the medium density FEMs that correlated poorly to the experimental results also had a high variability in the mean element ratio quality between blades. While hexahedral elements scale well in aspect ratio they are highly sensitive to skewing or warping, which can be introduced when displacing surface and interior nodes without considering mesh quality. Given that FEMs #5 and #6 began with high aspect ratio elements due to an unintentional artifact of the model generation process, even the smallest of node displacements were sufficient to warp or skew the mesh by such a degree as to introduce numerical mistuning. While these blade alone results could be considered within tolerance for a single blade harmonic analysis, they are insufficiently accurate for mistuning analysis given the

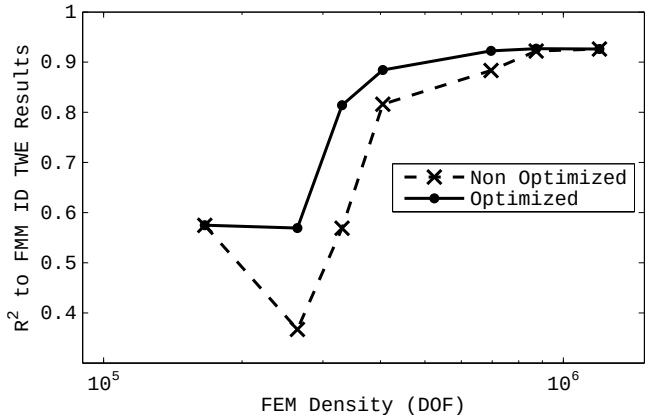

FIGURE 6: Accuracy Improvement with Mesh Quality Maintenance

sensitivity of IBR blade amplification due to mistuning. While these mesh inconsistencies were dampened in the higher density model #7, they were not eliminated and it remains part of the error of the analytical prediction given that the mesh variation still exists regardless of the mesh density and original aspect ratio. It is apparent that the original mesh updating scheme, while effective at capturing surface geometry, needs additional mesh optimization to obtain greater correlation with the experimental TWE results as to operate independently of the seed mesh shape and quality.

The analysis was rerun for STL # 5 and all FEMs. As shown in Figure 6 after the implementation of the mesh quality tracking and GETMe optimization scheme the accuracy of the results becomes more strongly correlated to FEM Density. One observation is the improvement in correlation to the experimental results drops for the high density FEM. As the element size falls, the contribution of interpolation error also falls but at a faster rate. Therefore, GETMe is critical for FEMs sensitive to mesh corruption but less useful for superdense FEMs or those relatively insensitive to mesh corruption. The parallel implementation of the GETMe algorithm and mesh quality tracking increased the computational cost of MORPH by 20%, and while it is useful for high aspect ratio hexahedral meshes, the computing time can be reduced by disabling GETMe for superdense meshes. However, the sequential, invalid element GETMe repair scheme has a minimal computational cost and is crucial for valid mesh generation.

Alignment Sensitivity Study

Point clouds obtained from optically scanned hardware do not begin with an initial datum alignment. On the contrary, these point clouds usually assume the scanner to be the origin of the scan volume. This complicates the MORPH process as the TSD must be registered to the seed FEM prior to adjusting the surface nodes of the FEM. The original MORPH algorithm utilized the iterative closest point (ICP) method which minimizes the mean squared error between the surface nodes of the FEM and the TSD. Given the non-uniform distribution of points on the optical scan data and its rigorous application on non-academic IBRs, it has become apparent that ICP applied to TSD can be sensitive to initial conditions and displays some hysteresis. A sensitivity study was conducted to determine the variability of accuracy given induced misalignment. Starting from an aligned position the IBR point cloud was translated by ± 60 mil ($\pm$ 1.524 mm) in the X and Z direction and $\pm 1^\circ$ deg about the X and Z axes. The IBR was aligned with the inlet of the IBR facing Z+ such that the Z axis is the vertical direction about which the rotor spins. The X and Y directions correspond to the radial direction in which the blades point. Results in the Y direction for both translation and rotation are excluded due to their similarity to X-axis results.

The results in Figure 7 indicates that sector mistuning is relatively insensitive to translation in the Z axis as this translation

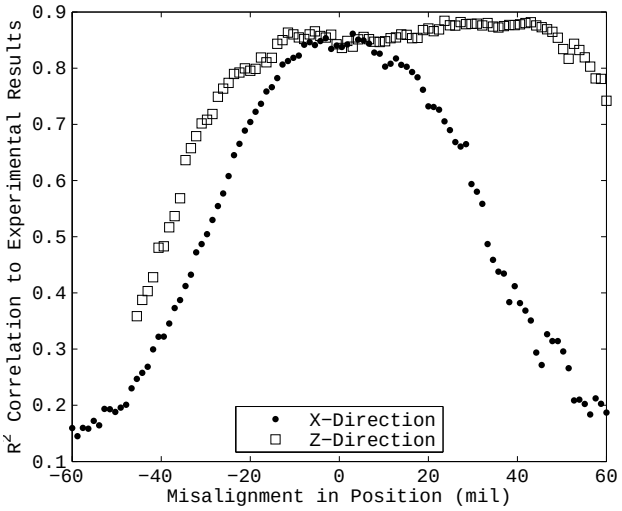

FIGURE 7: Accuracy to Experimental Results Given Translational Alignment Error

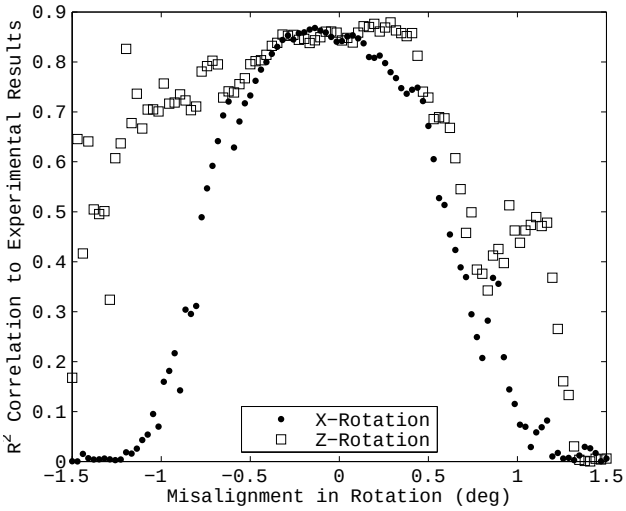

FIGURE 8: Accuracy to Experimental Results Given Rotational Alignment Error

direction does not effect relative blade geometric deviations. As disk nodes are kept fixed, the Z-position of the blades on the disk of the IBR changed when the TSD was shifted along the Z-axis, but as all blades were shifted the same distance this meant that the relative geometric variations remained constant. The low sensitivity to translation along the Z-axis from the ranges of -10 to $+50$ mil (-0.254 to $+1.27$ mm) is indicative of the robustness and accuracy of the MORPH algorithm despite the narrow thickness of the blades. This accuracy is due mainly to the intelligent neural network based node-TSD face pairing rather than direct node normal movement. The FEM displayed a greater sensitivity to X-axis translation but still had a relatively large range of insensitivity of ± 10 mil ($\pm 254\,\mu$m). Outside this range the accuracy of the mistuned model falls rapidly as this translation changes the relative blade lengths and positioning on the IBR. While minimum alignment ranges appear narrow when normalized by the diameter of the IBR $\pm 1.25 \times 10^{-4}$ % in x-axis translation, the actual variation in rotor positioning was less than $\pm$ 1 mil ($\pm 25.4\,\mu$m) in all dimensions. This was determined by repeatably aligning the rotor from various initial positions.

The variation in rotation about the X-axis had a significant effect on the accuracy of the GMM. The maximal tip displacement limit was $\pm$ 34 mil (0.864 mm) given that the region of sensitivity for the rotational displacement was $\pm 0.6^\circ$.

The range of insensitivity for Z-axis rotation was approximately $\pm 0.35^\circ$. This was confirmed by examining the GMM when the TSD was rotated beyond 0.35° about the Z-axis and finding that the nodes at the blades tip failed to update as the MORPH algorithm determined that there was insufficient agreement with the direction and normal alignment between the TSD and FEM. The rotational range of insensitivity is quite large considering that a displacement of 0.35° caused the blade tips to be displaced more than their thickness from the nominal FEM and is another demonstration on how MORPH is able to adapt to misalignment between the FEM and TSD. In practice ICP axial misalignment rarely exceeds $\pm 0.025^\circ$ according to repeated applications of the ICP algorithm from various initial conditions. The X-axis alignment results indicate a more narrow range of insensitivity as X-axis rotational alignment causes significant changes in the relative blade positioning and therefore a shift in blade to blade coupling and the tuned system frequencies. The smooth Gaussian distribution of correlations with the experimental results and centering of the results around the ICP solution indicate that ICP has converged on an accurate alignment to the seed FEM.

Two conclusions can also be inferred from these results and their distributions. First, FMM ID of both the TWE and GMM results have their correlations based primary in geometry as deviations from the ideal aligned case corrupt the correlations between the datasets. Second, the smooth distribution of results show that the MORPH algorithm is able to adapt to large variations in geometry and reflect those changes in the GMM's mistuned system modes.

Noise/Bias Sensitivity Study

Past research into the accuracy and repeatability of optical scanning systems has revealed has revealed that a $350 \times 280 \times 280$ mm optical scan volume has a 0.3 mil ($\pm 7.62\,\mu$m) variation between repeated scans of a scan target [10, 20]. While the scan volume used for this GMM is $175 \times 140 \times 135$ and has demonstrated a 0.16 mil ($\pm 4.06\,\mu$m) variation in surface geometry in repeated scans, no investigation was made into the effect of noise

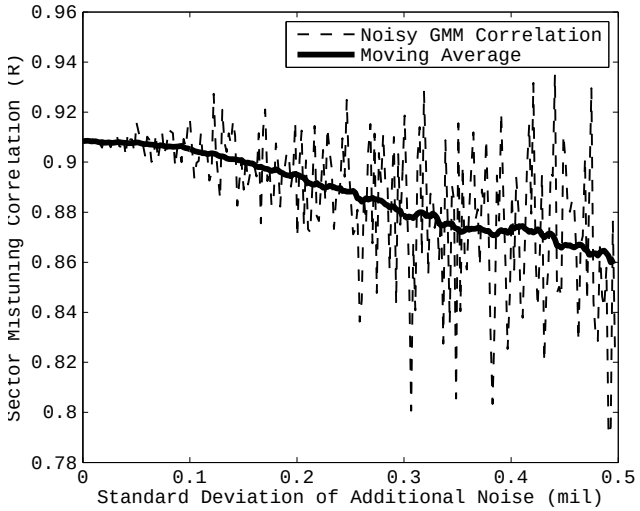

FIGURE 9: FEM Accuracy to Experimental Results Given Induced Noise

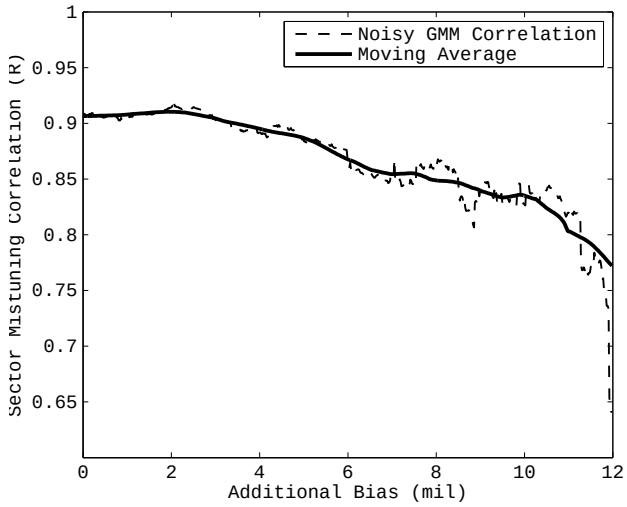

FIGURE 10: Accuracy to Experimental Results Given Bias

on the accuracy of a GMM. To determine this, an existing TSD containing 4 million geometric points of as-manufactured IBR was artificially seeded with noise to determine the variation in GMM accuracy given pseudo-noise.

Noise was introduced into the TSD by modifying each 3D point along its existing normal vector with cloud of normally distributed random displacements. The standard deviation of the normal distribution was varied from 0 to 0.5 mil (12.7 µm) to reflect a reasonable range of noise given fine and coarse point clouds collected from modern optical scanners. The results of 250 separate FEA analyses in Figure 9 indicate the accuracy of the GMM decreases with the introduction of noise into the TSD. The GMM accuracy can be expected to drop from 0.908 to 0.895 for the level of noise expected from the scan volume. This is a 1.43% drop in GMM accuracy from the ideal noiseless case and indicates that noise is a source of error that contributes to the variation between the TWE and GMM sector mistuning results. This analysis shows that noise is a significant contributor to solution accuracy and should be minimized when possible.

While the point resolution of an optical scanner accounts for the minimum optical noise, part reflectivity significantly contributes to scanner accuracy or the lack thereof. Objects that reflect rather than disperse light create ghost images and corrupts structured light patterns projected from the optical scanner. One approach to increase light dispersal from a part is to apply a thin coating of a light dispersing material such as Titanium Dioxide to the surface of the part. While TIO_2 can be applied as thin as [20] 0.0393 mil (1 µm), in practice actual applications can be orders of magnitude thicker and can vary in thickness depending on the method of application. Though advanced techniques can include applying the coating with a wide brush and then removing it to leave the thinnest possible residue, it can be difficult to determine the actual thickness of the coating left behind as well as its effect on the GMM and the FEA. MORPH cannot delineate between the coating and the part and the coating is treated as the part itself, potentially affecting the sector mistuning ratios within the GMM.

The effect of the thickening of the TSD was assessed by adding a consistent pseudo coating to the TSD by moving the points of the TSD outward along their node normals. The additional coating thickness ranged between 0 and 12 mil (0.3048 mm), a reasonable range considering the variability of coating applications due to the coating material and application method.

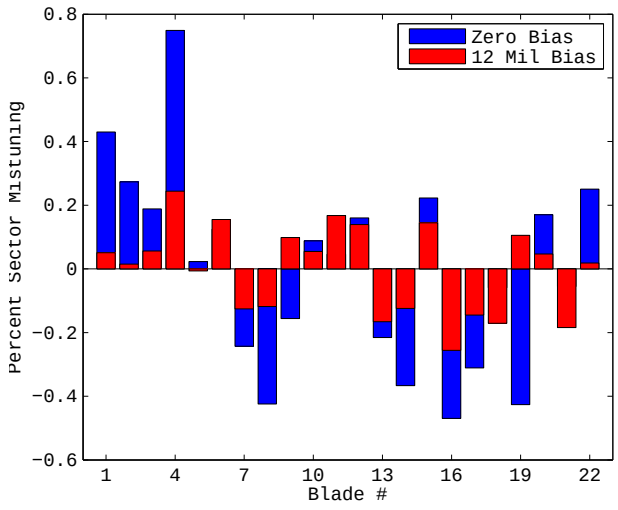

FIGURE 11: Relative Sector Mistuning With Nominal and +12 Mil Bias

Figure 10 shows the variation in sector mistuning accuracy due to the additional bias added to the TSD. Keeping in mind that this bias is added uniformly and does reduce the noise of the existing IBR, it appears that a thin coating has a minimal effect on the sector mistuning correlation. However, biases greater than 3 mil (76.2 µm) have a detrimental effect on the IBR as a 10 mil bias (0.254 mm) incurs a 7.49% reduction in accuracy and a 12 mil bias (0.3048 mm) incurs a severe 28.4% reduction in accuracy. Investigation into the GMM revealed that increasing thickness of the rotor had the greatest effect on the blade/disk interface. The greater fillet thickness increased the blade to disk coupling and decreased the blade vibrational energy. This decreased the relative blade mistuning ratios as shown in Figure 11. This would lead to a much more conservative estimate of relative blade mistuning as decreased mistuning ratios would reduce the likelihood of blade amplification and modal energy confinement. These results indicate that the additional anti-reflective coating should be kept as thin as possible.

More research needs to be conducted into measuring the actual thickness of applied coatings and measure the relative difference in noise caused by light scatter as well as additional TSD bias induced by an applied coating. However, it would appear from these results that a coating thickness of less than 3 mil (76.2 µm) has no detrimental effects on the accuracy of the GMM.

CONCLUSION

MORPH has been shown to be generate a valid GMM for an IBR given its strong agreement with experimental data and rigorous testing using multiple input variables. Bounds on optical scan noise, bias, point cloud density, as well as alignment accuracy have been established and shown to have a significant impact on mistuning prediction accuracy given experimental results. However, despite the sensitive nature of the GMM and its correlation to the experimental results, the MORPH algorithm exhibits the robustness and fidelity necessary for the reproduction of an IBR in the digital realm. This research also demonstrates the effects of numerical mistuning and how it can obscure actual rotor mistuning given variations in mesh quality throughout an IBR FEM. Major improvements to the algorithm have taken place to include the localized element quality verification the utilization of the GETMe algorithm to improve and correct the post-MORPH GMM element quality.

Additional research still needs to be conducted in establishing error bounds for the TWE by running repeated rotors scans and verifying the invariance of the results through FMM ID or establishing an error bound on TWE response prediction. MORPH should also be run on a population of production IBRs and compared to the experimental results to determine its accuracy across a population of IBRs while utilizing the same seed IBR.

MORPH has great potential for future GMM generation but also has a wide range of uses. It has also already been used modify "hot" tuned geometry to match cold optical scanning without user intervention to improve element quality, and these models have been used to generate accurate models for blade tip timing limits. Additionally, it has used to MORPH large individual fan blades meshed with tetrahedrals to compute as-manufactured mode shape for strain gauge placement. While more experimental validation will be useful to verify the absence of numerical mistuning and the accuracy of MORPH, thus far the MORPH algorithm has proven itself to be robust and accurate for both complex bladed assemblies and individual blades.

REFERENCES

[1] Castanier, M., and Pierre, C., 2006. "Modeling and analysis of mistuned bladed disk vibration: Current status and emergin directions". *Journal of Propulsion and Power,* ***22***(2).

[2] Bladh, R., Castanier, M., and Pierre, C., 2001. "Component-mode-based reduced order modeling techniques for mistuned bladed disks-part ii: Application,". *Journal of Engineering for Gas Turbines and Power,* ***123***(1), pp. 100–108.

[3] Yang, M., and Griffin, J., 1999. "A reduced-order model of mistuning using a subset of nominal system modes". *Journal of Engineering for Gas Turbines and Power,* ***123***(4), pp. 893–900.

[4] Beck, J., Brown, J., Slater, J., and Cross, C., 2012. "Probabilistic mistuning assessment using nominal and geometry based mistuning methods". *Journal of Turbomachinery,* ***135***(5), October.

[5] Beck, J., Brown, J., Slater, J., and Cross, C., 2013. "Probabilistic mistuning assessment using nominal and geometry based mistuning methods". *Journal of Turbomachinery,* ***135***(5).

[6] Sinha, A., Hall, B., Cassenti, B., and Hilbert, G., 2008. "Vibratory parameters of blades from coordinate measurement machine data". *Journal of Turbomachinery,* ***130***(1).

[7] Kaszynski, A., Beck, J., and Brown, J., 2014. "Automated finite element model mesh updating scheme applicable to mistuning analysis". In ASME Turbo Expo.

[8] Feiner, D., and Griffin, J., 2004. "Mistuning identification of bladed disks using a fundamental mistuning model-part i: Theory". *Journal of Turbomachinery,* ***126***(1), March, pp. 150–158.

[9] Feiner, D., and Griffin, J., 2004. "Mistuning identification of bladed disks using a fundamental mistuning modepart ii: Application". *Journal of Turbomachinery,* ***126***(1), March, pp. 159–165.

[10] Kaszynski, A., Beck, J., and Brown, J., 2013. "Uncertainties of an automated optical 3d geometry measurement, modeling, and analysis process for mistuned inte-

grally bladed rotor reverse engineering". *Journal of Engineering for Gas Turbines and Power,* ***135***.

[11] Moller, T., and Trumbore, B., 1997. "Fast, minimum storage ray-triangle intersection". *Journal of Graphics Tools,* ***2***, pp. 21–28.

[12] Liu, A., and Joe, B., 1994. "Relationship between tetrahedron shape measures". *BIT Numerical Mathematics,* ***34***(2), pp. 268–287.

[13] Freitag, L., Patrick, D., and Shontz, M. S. A comparison of two optimization methods for mesh quality improvement.

[14] Huang, W. "Measuring mesh qualities and application to variational mesh adaptation". *SIAM J. Sci. Comput*, pp. 1643–1666.

[15] Vollmer, J., Mencl, R., and Mller, H., 1999. "Improved laplacian smoothing of noisy surface meshes". In Computer Graphics Forum, pp. 131–138.

[16] Knupp, P., 2010. "Introducing the target-matrix paradigm for mesh optimization via node-movement". In *Proceedings of the 19th International Meshing Roundtable*, S. Shontz, ed. pp. 67–83.

[17] Vartziotis, D., and Wipper, J., 2012. "Fast smoothing of mixed volume meshes based on the effective geometric element transformation method". *Computer Methods for Applied Mechanical Engineering,* ***201-204***, pp. 65–81.

[18] Jones, K., and Cross, C., 2003. "Traveling wave excitation system for bladed disks". *Journal of Propulsion and Power,* ***19***.

[19] Munson, T., 2007. "Mesh shape-quality optimization using the inverse mean-ratio metric". *Mathematical Programming,* ***110***(3), pp. 561–590.

[20] Brajlih, T., Tasic, T., Drstvensek, I., Valentan, B., and Hadzistevic, M., 2011. "Possiblities of using threedimential optical scanning in complex geometrical inspection". *Journal of Mechanical Engineering,* ***57***, pp. 826–833.